Supporting Information

Xu et al. 10.1073/pnas.1301201110

SI Materials and Methods

1. Molecular Cloning. The *ccradS1* highly reducing iterative polyketide synthase (hrPKS) and the *ccradS2* nonreducing iterative polyketide synthase (nrPKS) genes were amplified separately using fosmid fCchi01A05 as the template (1). The two exons of *ccradS1* were amplified with the primer pairs RADS1_Up_F (NdeI) and RADS1_Up_R and RADS1_Dn_F and RADS1_Dn_R (PmeI). The resulting 3,957- and 3,375-bp products were fused by PCR using primers RADS1_Up_F (NdeI) and RADS1_Dn_R (PmeI), and the fused product was cloned into pJET1.2. After sequence verification, the *Nde*I-*Pme*I fragment was inserted into the same cloning sites of YEpADH2p-FLAG-TRP to yield YEpCcRADS1. The single exon of *ccradS2* was amplified using primers RADS2_F (NdeI) and RADS2_R (PmeI) to give a 6,439-bp product and cloned into pJET1.2. After sequence verification, the *Nde*I-*Pme*I fragment was inserted into the same sites of YEpADH2p-FLAG-URA to generate plasmid YEpCcRADS2.

The construction of the YEpAtCURS1 and YEpAtCURS2 expression plasmids with the *atcurS1* and *atcurS2* genes for the dehydrocurvularin hrPKS and nrPKS, respectively, followed a similar scheme and has been described.

The Udwary–Merski algorithm was used to predict domain boundaries in nrPKS (2).

YEpAtCURS2-ΔPT is based on YEpADH2p-FLAG-URA and carries the intronless *atcurS2* gene with the product template (PT) domain deleted (Pro^{1270} to Ser^{1614}). Using YEpAtCURS2 as the template, 470- and 1,046-bp PCR products were generated by PCR using primers At_PT_Del_Up_F (AgeI) and At_PT_Del_UP_R and At_PT_Del_Dn_F and At_PT_Del_Dn_R (NheI), respectively. These PCR products were fused by overlap extension PCR using primers At_PT_Del_Up_F and At_PT_Del_Dn_R. The resulting 1,516-bp PCR product was cloned into pJET1.2 and verified by sequencing, and the *Age*I-*Nhe*I fragment was inserted into the same cloning sites of YEpATCURS2 to yield plasmid YEpATCURS2-ΔPT.

YEpCcRADS2-ΔPT is based on YEpADH2p-FLAG-URA and carries the intronless *ccradS2* gene with the PT domain deleted (Gln^{1284} to Thr^{1640}). Using YEpCcRADS2 as the template, 360- and 1,388-bp PCR products were generated by PCR using primers Cc_PT_Del_Up_F (Bsu36I) and Cc_PT_Del_Up_R and Cc_PT_Del_Dn_F and Cc_PT_Del_Dn_R (BglII), respectively. These PCR products were fused by overlap extension PCR using primers Cc_PT_Del_Up_F and Cc_PT_Del_Dn_R. The resulting 1,748-bp PCR product was cloned into pJET1.2 and verified by sequencing, and the *Bsu*36I-*Bgl*II fragment was inserted into the same cloning sites of YEpCcRADS2 to yield plasmid YEpCcRADS2-ΔPT.

YEpAtCURS2-ΔPT+$PT_{AtCURS2}$ is based on YEpADH2p-FLAG-URA and carries both the PT domain-deleted *atcurS2* gene and a separate gene encoding $PT_{AtCURS2}$ driven by separate copies of the alcohol dehydrogenase (ADH2) promoter. Using YEpAtCURS2 as the template, a 683-bp ADH2 promoter fragment, the 1,060-bp $PT_{AtCURS2}$ gene fragment, and a 469-bp ADH2 terminator fragment were separately amplified with primers At_PT_p_F (KpnI), At_PT_p_R, At_PT_F, and At_PT_R and At_PT_t_F and At_PT_t_R (HpaI), respectively. These PCR products were fused by overlap extension PCR using primers At_PT_p_F (KpnI) and At_PT_t_R (HpaI) and cloned into pJET1.2. After sequence verification, the *Kpn*I-*Hpa*I fragment was inserted into the same cloning sites of YEpATCURS2-ΔPT to yield plasmid YEpAtCURS2-ΔPT+$PT_{AtCURS2}$.

YEpCcRADS2-ΔPT+$PT_{CcRADS2}$ is based on YEpADH2p-FLAG-URA and carries both the PT domain-deleted *ccradS2* gene and a separate gene encoding $PT_{CcRADS2}$ driven by separate copies of the ADH2 promoter. Using YEpCcRADS2 as the template, a 655-bp ADH2 promoter fragment, the 1,101-bp $PT_{CcRADS2}$ gene fragment, and a 392-bp ADH2 terminator fragment were separately amplified with primers Cc_PT_p_F (EcoRI) and Cc_PT_p_R, Cc_PT_F and Cc_PT_R, and Cc_PT_t_F and Cc_PT_t_R (HpaI), respectively. These PCR products were fused by overlap extension PCR using primers Cc_PT_p_F (EcoRI) and Cc_PT_t_R (HpaI) and cloned into pJET1.2. After sequence verification, the *EcoR*I-*Hpa*I fragment was inserted into the same cloning sites of YEpCcRADS2-ΔPT to yield plasmid YEpCcRADS2-ΔPT+$PT_{CcRADS2}$.

The plasmid YEpAtCURS2-$PT_{CcRADS2}$, in which the gene segment encoding $PT_{AtCURS2}$ was replaced by the one encoding $PT_{CcRADS2}$, was constructed using the following steps. A 471-bp upstream fragment encoding P^{1120}-G^{1269} of AtCURS2 was amplified with primers At_PT_Del_Up_F (AgeI) and At_PT_Up_R. A 1,094-bp fragment encoding CcRADS2 Q^{1284}-T^{1640} was amplified with primers Cc_PT_to_At_F and Cc_PT_to_At_R. A 1,046-bp downstream fragment encoding S^{1614}-A^{1961} of AtCURS2 was amplified with primers At_PT_Del_Dn_F and At_PT_Del_Dn_R (NheI). These three PCR fragments were then fused using primers At_PT_Del_Up_F (AgeI) and At_PT_Del_Dn_R (NheI) and cloned into pJET1.2, and the sequence was verified. Finally, the *Age*I-*Nhe*I fragment was inserted into the same cloning sites of YEpATCURS2 to yield plasmid YEpAtCURS2-$PT_{CcRADS2}$.

The plasmid YEpCcRADS2-$PT_{AtCURS2}$, in which the gene segment encoding $PT_{CcRADS2}$ was replaced by the one encoding $PT_{AtCURS2}$, was constructed using the following steps. A 378-bp upstream fragment encoding L^{1165}-A^{1284} of CcRADS2 was amplified with primers Cc_PT_Del_Up_F (Bsu36I) and Cc_PT_Up_R. A 1,051-bp fragment encoding AtCURS2 P^{1270}-V^{1613} was amplified with primers At_PT_to_Cc_F and At_PT_to_Cc_R. A 1,388-bp downstream fragment encoding P^{1642}-C^{2103} of CcRADS2 was amplified with primers Cc_PT_Del_Dn_F and Cc_PT_Del_Dn_R (BglII). These three PCR fragments were then fused using primers Cc_PT_Del_Up_F (Bsu36I) and Cc_PT_Del_Dn_R (BglII) and cloned into pJET1.2, and the sequence was verified. Finally, the *Bsu*36I-*Bgl*II fragment was inserted into the same cloning sites of YEpCcRADS2 to yield plasmid YEpCcRADS2-$PT_{AtCURS2}$.

The mutation encoding the $F^{1459}Y$ change was introduced into *atcurS2* by replacing the F^{TTC} codon with Y^{TAC}. A 1,038-bp upstream fragment was amplified using primers At_PT_Del_Up_F (AgeI) and Phe198Y_R, and a 1,531-bp downstream fragment was generated with primers Tyr319F_F and At_PT_Del_Dn_R (NheI). The two PCR products were fused using the At_PT_Del_Up_F (AgeI) and the At_PT_Del_Dn_R (NheI) primers, and the fragment was cloned into pJET1.2. After sequence verification, the *Age*I-*Nhe*I fragment was inserted into the same cloning sites of YEpAtCURS2 to yield plasmid YEpAtCURS2($F^{1459}Y$).

The mutation encoding the $Y^{1576}F$ change was introduced into *atcurS2* by replacing the Y^{TAT} codon with F^{TTT}. A 1,390-bp upstream fragment was amplified using primers At_PT_Del_Up_F (AgeI) and TYR319F_R, and a 1,157-bp downstream fragment was generated with primers Trp327_F and At_PT_Del_Dn_R (NheI). The two PCR products were fused using the At_PT_Del_Up_F (AgeI) and the At_PT_Del_Dn_R (NheI) primers, and the fragment was cloned into pJET1.2. After sequence verification, the *Age*I-*Nhe*I fragment was inserted into the same cloning sites of YEpAtCURS2 to yield plasmid YEpAtCURS2($Y^{1576}F$).

The mutation encoding the $W^{1584}L$ change was introduced into *atcurS2* by replacing the W^{TGG} codon with L^{TTG}. A 1,393-bp upstream fragment was amplified using primers At_PT_Del_Up_F (AgeI) and Phe198Tyr319_R, and a 1,153-bp downstream fragment was generated with primers Trp327L_F -3′ and At_PT_Del_Dn_R (NheI). The two PCR products were fused using the At_PT_Del_Up_F (AgeI) and the At_PT_Del_Dn_R (NheI) primers, and the fragment was cloned into pJET1.2. After sequence verification, the *Age*I-*Nhe*I fragment was inserted into the same cloning sites of YEpAtCURS2 to yield plasmid YEpAtCURS2($W^{1584}L$).

The double mutation encoding the $F^{1459}Y$ and $Y^{1576}F$ change was introduced into *atcurS2* by replacing the F^{TTC} codon with Y^{TAC} and the Y^{TAT} codon with F^{TTT}. A 1,038-bp upstream fragment was amplified using primers At_PT_Del_Up_F (AgeI) and Phe198Y_R, a 393-bp middle fragment was generated with primers Tyr319F_F and Tyr319F_R, and a 1,157-bp downstream fragment was amplified with primers Trp327_F and At_PT_Del_Dn_R (NheI). The three PCR products were fused using the At_PT_Del_Up_F (AgeI) and At_PT_Del_Dn_R (NheI) primers, and the fragment was cloned into pJET1.2. After sequence verification, the *Age*I-*Nhe*I fragment was inserted into the same cloning sites of YEpAtCURS2 to yield plasmid YEpAtCURS2($F^{1459}Y$,$Y^{1576}F$).

The double mutation encoding the $F^{1459}Y$ and $W^{1584}L$ change was introduced into *atcurS2* by replacing the F^{TTC} codon with Y^{TAC} and the W^{TGG} codon with L^{TTG}. A 1,038-bp upstream fragment was amplified using primers At_PT_Del_Up_F (AgeI) and Phe198Y_R, a 393-bp middle fragment was generated with primers Tyr319F_F and Y319_R, and a 1,153-bp downstream fragment was amplified with primers Trp327L_F and At_PT_Del_Dn_R (NheI). The three PCR products were fused using the At_PT_Del_Up_F (AgeI) and At_PT_Del_Dn_R (NheI) primers, and the fragment was cloned into pJET1.2. After sequence verification, the *Age*I-*Nhe*I fragment was inserted into the same cloning sites of YEpAtCURS2 to yield plasmid YEpAtCURS2($F^{1459}Y$,$W^{1584}L$).

The double mutation encoding the $Y^{1576}F$ and $W^{1584}L$ change was introduced into *atcurS2* by replacing the Y^{TAT} codon with F^{TTT} and the W^{TGG} codon with L^{TTG}. A 1,390-bp upstream fragment was amplified using primers At_PT_Del_Up_F (AgeI) and Tyr319F_R, and a 1,153-bp downstream fragment was generated with primers Trp327L_F and At_PT_Del_Dn_R (NheI). The two PCR products were fused using the At_PT_Del_Up_F (AgeI) and At_PT_Del_Dn_R (NheI) primers, and the fragment was cloned into pJET1.2. After sequence verification, the *Age*I-*Nhe*I fragment was inserted into the same cloning sites of YEpAtCURS2 to yield plasmid YEpAtCURS2($Y^{1576}F$,$W^{1584}L$).

The triple mutation encoding the $F^{1459}Y$, $Y^{1576}F$, and $W^{1584}L$ change was introduced into *atcurS2* by replacing the F^{TTC} codon with Y^{TAC}, the Y^{TAT} codon with F^{TTT}, and the W^{TGG} codon with L^{TTG}. A 1,038-bp upstream fragment was amplified using primers At_PT_Del_Up_F (AgeI) and Phe198Y_R, a 393-bp middle fragment was generated with primers Tyr319F_F and Y319F_R, and a 1,153-bp downstream fragment was generated with primers Trp327L_F and At_PT_Del_Dn_R (NheI). The three PCR products were fused using the At_PT_Del_Up_F (AgeI) and At_PT_Del_Dn_R (NheI) primers, and the fragment was cloned into pJET1.2. After sequence verification, the *Age*I-*Nhe*I fragment was inserted into the same cloning sites of YEpAtCURS2 to yield plasmid YEpAtCURS2($Y^{1576}F$,$Y^{1576}F$,$W^{1584}L$).

The mutation encoding the $Y^{1483}F$ change was introduced into *ccradS2* by replacing the Y^{TAC} codon with F^{TTC}. A 976-bp upstream fragment was amplified using primers Cc_PT_Del_Up_F (Bsu36I) and Y209F_R, and a 1,864-bp downstream fragment was generated with primers Y209_F and Cc_PT_Del_Dn_R (BglII). The two PCR products were fused using the Cc_PT_Del_Up_F (Bsu36I) and Cc_PT_Del_Dn_R (BglII) primers, and the fragment was cloned into pJET1.2. After sequence verification, the *Bsu*36I-*Bgl*II fragment was inserted into the same cloning sites of YEpCcRADS2 to yield plasmid YEpCcRADS2($Y^{1483}F$).

The mutation encoding the $F^{1602}Y$ change was introduced into *ccradS2* by replacing the F^{TTC} codon with Y^{TAC}. A 1,332-bp upstream fragment was amplified using primers Cc_PT_Del_Up_F (Bsu36I) and F332Y_R, and a 1,506-bp downstream fragment was generated with primers F332_F and Cc_PT_Del_Dn_R (BglII). The two PCR products were fused using the Cc_PT_Del_Up_F (Bsu36I) and Cc_PT_Del_Dn_R (BglII) primers, and the fragment was cloned into pJET1.2. After sequence verification, the *Bsu*36I-*Bgl*II fragment was inserted into the same cloning sites of YEpCcRADS2 to yield plasmid YEpCcRADS2($F^{1602}Y$).

The mutation encoding the $L^{1610}W$ change was introduced into *ccradS2* by replacing the L^{CTG} codon with W^{TGG}. A 1,335-bp upstream fragment was amplified using primers Cc_PT_Del_Up_F (Bsu36I) and L340_R, and a 1,504-bp downstream fragment was generated with primers L340W_F and Cc_PT_Del_Dn_R (BglII). The two PCR products were fused using the Cc_PT_Del_Up_F (Bsu36I) and Cc_PT_Del_Dn_R (BglII) primers, and the fragment was cloned into pJET1.2. After sequence verification, the *Bsu*36I-*Bgl*II fragment was inserted into the same cloning sites of YEpCcRADS2 to yield plasmid YEpCcRADS2($L^{1610}W$).

The double mutation encoding the $Y^{1483}F$ and $F^{1602}Y$ change was introduced into *ccradS2* by replacing the Y^{TAC} codon with F^{TTC} and the F^{TTC} codon with Y^{TAC}. A 976-bp upstream fragment was amplified using primers Cc_PT_Del_Up_F (Bsu36I) and Y209F_R, a 376-bp middle fragment was generated with primers Y209_F and F332Y_R, and a 1,506-bp downstream fragment was generated with primers F332_F and Cc_PT_Del_Dn_R (BglII). The three PCR products were fused using the Cc_PT_Del_Up_F (Bsu36I) and Cc_PT_Del_Dn_R (BglII) primers, and the fragment was cloned into pJET1.2. After sequence verification, the *Bsu*36I-*Bgl*II fragment was inserted into the same cloning sites of YEpCcRADS2 to yield plasmid YEpCcRADS2($Y^{1483}F$, $F^{1602}Y$).

The double mutation encoding the $F^{1602}Y$ and $L^{1610}W$ change was introduced into *ccradS2* by replacing the F^{TTC} codon with Y^{TAC} and the L^{CTG} codon with W^{TGG}. A 1,332-bp upstream fragment was amplified using primers Cc_PT_Del_Up_F (Bsu36I) and F332Y_R, and a 1,504-bp downstream fragment was generated with primers L340W_F and Cc_PT_Del_Dn_R (BglII). The two PCR products were fused using the Cc_PT_Del_Up_F (Bsu36I) and Cc_PT_Del_Dn_R (BglII) primers, and the fragment was cloned into pJET1.2. After sequence verification, the *Bsu*36I-*Bgl*II fragment was inserted into the same cloning sites of YEpCcRADS2 to yield plasmid YEpCcRADS2($F^{1602}Y$,$L^{1610}W$).

The double mutation encoding the $Y^{1483}F$ and $L^{1610}W$ change was introduced into *ccradS2* by replacing the Y^{TAC} codon with F^{TTC} and the L^{CTG} codon with W^{TGG}. A 976-bp upstream fragment was amplified using primers Cc_PT_Del_Up_F (Bsu36I) and Y209F_R, a 379-bp middle fragment was generated with primers Y209_F and L340_R, and a 1,504-bp downstream fragment was generated with primers L340W_F and Cc_PT_Del_Dn_R (BglII). The three PCR products were fused using the Cc_PT_Del_Up_F (Bsu36I) and Cc_PT_Del_Dn_R (BglII) primers, and the fragment was cloned into pJET1.2. After sequence verification, the *Bsu*36I-*Bgl*II fragment was inserted into the same cloning sites of YEpCcRADS2 to yield plasmid YEpCcRADS2($Y^{1483}F$,$L^{1610}W$).

The triple mutation encoding the $Y^{1483}F$, $F^{1602}Y$, and $L^{1610}W$ change was introduced into *ccradS2* by replacing the Y^{TAC} codon with F^{TTC}, the F^{TTC} codon with Y^{TAC}, and the L^{CTG} codon with W^{TGG}. A 976-bp upstream fragment was amplified using primers At_PT_Del_Up_F (AgeI) and Y209F_R, a 376-bp middle fragment was generated with primers Y209_F and F332Y_R, and a 1,504-bp downstream fragment was generated with primers L340W_F and Cc_PT_Del_Dn_R (BglII). The three PCR products were fused using the Cc_PT_Del_Up_F (Bsu36I) and Cc_PT_Del_Dn_R (BglII) primers, and the fragment was cloned into pJET1.2. After sequence verification, the *Bsu*36I-*Bgl*II fragment

was inserted into the same cloning sites of YEpCcRADS2 to yield plasmid YEpCcRADS2($Y^{1483}F$,$F^{1602}Y$,$L^{1610}W$).

2. Heterologous Production and Isolation of Polyketides. ***Large-scale fermentation and isolation of products.*** For a typical large-scale fermentation process, 20 250-mL Erlenmeyer flasks, each containing 50 mL 0.67% (wt/vol) yeast nitrogen base, 2% (wt/vol) glucose, and 0.72 g/L Trp/Ura DropOut medium, were inoculated with the appropriate yeast strain and cultivated at 30 °C with shaking at 300 rpm. After the OD_{600} reached 1.0, 50 mL 1% (wt/vol) yeast extract and 2% (wt/vol) peptone (YP) medium was added to each flask, and the cultivation was continued for 3 d. The culture was centrifuged at 2,500 × *g* for 5 min to remove the yeast cells, and the supernatant was concentrated to 200 mL using a rotary evaporator. The concentrated broth was adjusted to pH 5.0 and extracted with 600 mL EtOAc three times. After evaporation of the solvent, the sample was loaded to a Diaion HP-20 column (4 × 30 cm) and successively eluted with H_2O, 25% MeOH/H_2O, and acetone. The acetone fraction was collected and further separated by HPLC using an Eclipse XDB C18 column (5 μm, 4.6 × 150 mm) and/or an Eclipse Plus C8 column (5 μm, 4.6 × 150 mm).

Compound **1** (monocillin II, 8.9 mg) was purified from the acetone fraction of the extract of *Saccharomyces cerevisiae* BJ5464-NpgA (YEpCcRADS1, YEpCcRADS2) by HPLC using an Eclipse XDB C18 column (52% CH_3CN/H_2O, 1 mL/min). Compound **2** (5.2 mg) was obtained by HPLC separation of the acetone fraction of the extract of *S. cerevisiae* BJ5464-NpgA (YEpAtCURS1, YEpAtCURS2) on an Eclipse XDB C18 column (41% CH_3CN/H_2O, 1 mL/min). Compounds **3** (3.1 mg) and **4** (3.2 mg) were purified from strain *S. cerevisiae* BJ5464-NpgA [YEpAtCURS1, YEpAtCURS2($F^{1455}Y$,$Y^{1576}F$,$W^{1584}L$)] by separation of the acetone fraction on an Eclipse XDB C18 column (39% CH_3CN/H_2O, 1 mL/min). Compound **5** (2.1 mg) was isolated from *S. cerevisiae* BJ5464-NpgA (YEpCcRADS1, YEpCcRADS2-$PT_{AtCURS2}$) by HPLC separation of the acetone fraction on an Eclipse XDB C18 column (33% CH_3CN/H_2O, 1 mL/min) and an Eclipse Plus C8 column (22% CH_3CN/H_2O, 1 mL/min).

Analysis of the time course of the production of 3 and 4. Erlenmeyer flasks (125 mL) containing 50 mL 0.67% yeast nitrogen base, 2% glucose, and 0.72 g/L Trp/Ura DropOut medium were inoculated with *S. cerevisiae* BJ5464-NpgA (YEpAtCURS1, YEpATCURS2-$PT_{CcRADS2}$), and the cultures were incubated at 30 °C with shaking at 250 rpm. When the OD_{600} reached 0.6 (referred to as 0 h in Fig. 3*A*), an equal volume of YP medium was added to the cultures, and the fermentation was continued at 30 °C with shaking at 250 rpm for an additional 3 d. One flask was harvested at 0, 24, 48, and 72 h after the addition of the YP medium, and the polyketide products were extracted and analyzed as described in *Materials and Methods*, *Small-Scale Fermentation and Analysis of Products*.

Biotransformation of 3 to 4 by* S. cerevisiae *BJ5464-NpgA. A 125 mL Erlenmeyer flask containing 20 mL yeast extract peptone dextrose agar (YPD) liquid medium was inoculated with the untransformed yeast host strain *S. cerevisiae* BJ5464-NpgA, and the culture was incubated overnight with shaking at 200 rpm at 30 °C. Two-milliliter aliquots of this starter culture were transferred to 250 mL Erlenmeyer flasks containing 50 mL fresh YPD medium each and cultured at 30 °C with shaking at 200 rpm for 3 h; 200 μg compound **3**, dissolved in 100 μL MeOH, were supplemented to each of the yeast cultures, and cultivation was continued at 30 °C with shaking at 200 rpm. One flask each was harvested at 0, 24, 48, and 72 h after the addition of **3** and extracted with an equal volume of ethyl acetate. The organic extracts were evaporated to dryness and analyzed by reversed-phase HPLC as described above. Controls consisted of **3** incubated for 72 h with shaking at 200 rpm at 30 °C in YPD medium that has not been inoculated with the yeast and a 72 h culture of *S. cerevisiae* BJ5464-NpgA without supplementation with **3**.

3. Chemical Characterization of Polyketide Products. Optical rotations were recorded on a Rudolph Autopol IV polarimeter with a 10-cm cell. Circular dichroism (CD) spectra were acquired with a JASCO J-810 instrument using a path length of 1 cm. ^1H, ^{13}C, and 2D NMR [homonuclear correlation spectroscopy (COSY), heteronuclear single-quantum correlation spectroscopy (HSQC), heteronuclear multiple-bond correlation spectroscopy (HMBC), and rotating frame nuclear Overhauser effect spectroscopy (ROESY)] spectra were recorded in DMSO-d_6, CD_3OD, or C_5D_5N on a JEOL ECX-300 Spectrometer [δ (ppm), *J* (Hz)]. ESI-MS data were collected on an Agilent 6130 Single Quad LC-MS.

Electrospray ionization mass spectrometry (ESI-MS) analysis revealed that the molecular weight of **1** (Fig. S2) is 316. A comparison of the retention time, UV spectrum (Fig. S5), and NMR data of **1** and authentic monocillin II (3) confirmed that they are identical.

ESI-MS of **2** showed the $[M+H]^+$ and $[M+Na]^+$ ion peaks at *m/z* 291.1 and 313.3, respectively, indicating that its molecular weight is 290. The ^1H NMR, ^{13}C NMR, and optical rotation data were in full agreement with the data reported in the literature for 10,11-dehydrocuvularin (4). Absolute configuration of C-15 was proved to be *S* by a comparison of the optical rotation and negative Cotton effect at 236 nm in the CD spectrum (Fig. S6) with the optical rotations and CD spectra of 15-*S*-dehydrocurvularin and 15-*R*-dehydrocurvularin (5, 6). Thus, **2** was identified as 15-*S*-dehydrocurvularin (Fig. S2).

ESI-MS of **3** revealed that its molecular weight is 290, the same as the molecular weight of **2**. The ^{13}C NMR spectra showed 16 carbon signals, indicating that **3** is also an octaketide. However, unlike **2**, **3** showed a characteristic isocoumarin UV absorption spectrum (Fig. S5), suggesting that it is an isocoumarin analog. Based on the 1D (Table S1) and 2D NMR spectra (Fig. S3), **3** was identified as 6,8-dihydroxy-3-(6-hydroxyhept-1-enyl)-1*H*-isochromen-1-one, an isocoumarin with a 7-carbon side chain containing a double bond and a hydroxyl group. The double bond was determined to be *E* based on the large coupling constant between H-10 and H-11 (15.8 Hz in pyridine-d_5 and 15.5 Hz in DMSO-d_6) (Table S1). Absolute configuration at C-15 in **3** was determined by Mosher's method. The Δδ-value (−0.02) of CH_3-16 (Fig. S4) confirmed that C-15 in **3** is in the *S* configuration. Thus, **3** was characterized as (*S*,*E*)-6,8-dihydroxy-3-(6-hydroxyhept-1-enyl)-1*H*-isochromen-1-one (Fig. S2).

ESI-MS revealed that the molecular weight of **4** is 288, two mass units less than the molecular weight of **3**. The UV spectrum (Fig. S5) suggested that **4** is also an isocoumarin. The ^{13}C NMR spectrum of **4** is similar to the spectrum of **3**, except that there is a keto group (δ 208.8) at C-15 instead of a hydroxyl. Based on the 1D (Table S1) and 2D NMR spectra (Fig. S3), **4** was identified as (*E*)-6,8-dihydroxy-3-(6-oxohept-1-enyl)-1*H*-isochromen-1-one (Fig. S2).

The $[M+H]^+$ (*m/z* 335.2) and $[M+Na]^+$ (*m/z* 373.1) ion peaks indicated that the molecular weight of **5** is 334. The ^1H-^1H COSY spectrum revealed the presence of a spin system (CH-CH_2-CH_2-CH = CH-CH_2-CH-CH_3) that contains two oxygenated methines at δ_H 4.32 (m, 1H) and 3.55 (m, 1H) and one double bond. The configuration of the $\Delta^{14,15}$ double bond was assigned as *E* according to the coupling constant ($J_{14/15}$ = 15.8 Hz in pyridine-d_5). The ^1H-^1H COSY and ROESY correlations of H-17 with OH-17 indicated the presence of a free hydroxyl group at C-17 (Figs. S3 and S7). Thus, the lactone bond was deduced to be formed between C-1 and C-11. The CD spectrum of **5** showed negative Cotton effect at 211 nm corresponding to the lactone bond (Fig. S6), which was consistent with 15-*S*-dehydrocurvularin derivatives and opposite to 15-*R*-dehydrocurvularin (5–7). Because the chiral carbon C-17 was not close enough to strongly affect the Cotton effect arising from the lactone bond (6), the absolute configuration of C-11 could be elucidated as 11*S*. Configuration at C-17 in **5** was established as 17*R* based on the Δδ-value (+0.08) using Mosher's

method (Fig. S4). Therefore, the structure of **5** was determined to be (*S*)-7,9-dihydroxy-4-((*R*,*E*)-6-hydroxyhept-3-enyl)-4,5-dihydro-1*H*-benzo[d]oxocine-2,6-dione (Fig. S2).

Monocillin II (**1**): colorless solid; ^{1}H NMR (300 MHz, pyridine-d_5): δ 6.90 (m, 1H), 6.85 (d, J = 1.8 Hz, 1H), 6.83 (d, J = 1.8 Hz, 1H), 6.11 (d, J = 15.8 Hz, 1H), 5.38 (dt, J = 16.1, 6.2 Hz, 1H), 5.27 (m, 1H), 5.17 (overlap, 1H), 4.29 (d, J = 16.2 Hz, 1H), 4.16 (d, J = 16.2 Hz, 1H), 2.54 (m, 1H), 2.17 (m, 1H), 2.03 (m, 4H), 1.30 (d, J = 6.5 Hz, 3H); ^{13}C NMR (75 MHz, pyridine-d_5): δ 197.3, 170.6, 164.6, 163.8, 147.9, 140.0, 132.3, 131.2, 128.5, 112.6, 108.8, 103.3, 72.4, 48.3, 38.1, 31.6, 31.5, 19.2; ESI-MS (−): $[M-H]^-$ m/z 315.1; ESI-MS (+): $[M+H]^+$ m/z 316.9.

10,11-Dehydrocurvularin (**2**): pale yellow amorphous solid; $[\alpha]_D^{23} = -23.8°$ (4.5 mM in MeOH); ^{1}H NMR (300 MHz, CD_3OD): δ 6.56 (m, 1H), 6.49 (d, J = 15.8 Hz, 1H), 6.29 (s, 1H), 6.25 (s, 1H), 4.75 (m, 1H), 3.69 (d, J = 16.5 Hz, 1H), 3.45(d, J = 16.5 Hz, 1H), 2.20–2.45 (m, 2H), 1.81–2.03 (m, 2H), 1.52–1.56 (m, 2H), 1.18 (d, J = 6.3 Hz, 3H); ^{13}C NMR (75 MHz, CD_3OD): δ 197.2, 172.5, 163.8, 160.9, 150.0, 138.5, 132.4, 116.5, 112.3, 102.2, 71.1, 41.6, 33.7, 32.9, 24.5, 19.1; CD: $\delta\varepsilon_{236}$ −2.32, $\delta\varepsilon_{300}$ −0.33, $\delta\varepsilon_{336}$ +0.16 (4.5 mM in MeOH); ESI-MS (−): $[M-H]^-$ m/z 289.1; ESI-MS (+): $[M+H]^+$ m/z 291.1, $[M+Na]^+$ m/z 313.3.

Compound **3**: pale yellow amorphous solid; $[\alpha]_D^{23} = +11.4°$ (1.2 mM in $CHCl_3$); ^{1}H and ^{13}C NMR in CD_3OD (Table S1); ^{1}H NMR (300 MHz, pyridine-d_5): δ 6.84 (d, J = 2.1 Hz, 1H), 6.71 (d, J = 2.1 Hz, 1H), 6.60 (dt, J = 15.8, 7.2 Hz, 1H), 6.37 (s, 1H), 6.11 (d, J = 15.8 Hz, 1H), 4.02 (m, 1H), 2.21 (m, 1H), 1.73 (m, 1H), 1.59 (m, 1H), 1.36 (d, J = 6.2 Hz, 1H); ESI-MS (−): $[M-H]^-$ m/z 289.1; ESI-MS (+): $[M+H]^+$ m/z 291.1, $[M+Na]^+$ m/z 313.1.

Compound **4**: white amorphous solid; ^{1}H and ^{13}C NMR (Table S1); ESI-MS (−): $[M-H]^-$ m/z 287.1; ESI-MS (+): $[M+H]^+$ m/z 289.1.

Compound **5**: white amorphous solid; $[\alpha]_D^{23} = -14.0°$ (1.5 mM in MeOH); ^{1}H and ^{13}C NMR in DMSO-d_6 (Table S1); ^{1}H NMR (300 MHz, pyridine-d_5): δ 6.94 (s, 1H), 6.80 (s, 1H), 5.72 (dt, J = 15.8, 7.2 Hz, 1H), 5.53 (dt, J = 15.8, 7.6 Hz, 1H), 4.57 (d, J = 17.9 Hz, 1H), 4.49 (d, J = 17.9 Hz, 1H), 4.40 (m, 1H), 4.06 (m, 1H), 2.66 (d, J = 7.6 Hz, 2H), 2.42 (m, 1H), 2.33 (m, 1H), 2.18 (m, 2H), 1.84 (m, 1H), 1.65 (m, 1H), 1.34 (d, J = 5.8 Hz, 3H); CD: $\delta\varepsilon_{211}$ −0.71, $\delta\varepsilon_{265}$ +0.01, $\delta\varepsilon_{278}$ +0.02, $\delta\varepsilon_{303}$ +0.03, $\delta\varepsilon_{333}$ −0.06 (3.1 mM in MeOH); ESI-MS (−): $[M-H]^-$ m/z 333.1; ESI-MS (+): $[M+H]^+$ m/z 335.2, $[M+Na]^+$ m/z 357.2, $[M+K]^+$ m/z 373.1.

1.4. Preparation of Mosher Ester Derivatives of 3 and 5. One-half milligram **3** or **5** was transferred into a clean and completely dry NMR tube. Deuterated pyridine (0.5 mL) and (*S*)-(+)-α-methoxy-α-(trifluoromethyl)phenylacetyl chloride [(*S*)-MTPA-Cl); 6 μL] were added to each NMR tube immediately, and the tubes were shaken carefully to evenly mix the sample with (*S*)-MTPA-Cl. The reaction mixtures were incubated at 15 °C for 12 h to yield the MTPA esters **3-S** and **5-S**, respectively. The esters **3-R** and **5-R** were obtained similarly by reacting **3** and **5** with (*R*)-MTPA-Cl, respectively.

Compound **3-S**: ^{1}H-NMR (300 MHz, pyridine-d_5): δ 6.95 (d, J = 2.2 Hz, 1H), 6.87 (d, J = 2.2 Hz, 1H), 6.53 (m, 1H), 6.34 (s, 1H), 6.08 (d, J = 15.7 Hz, 1H), 3.65 (m, 2H), 2.19–1.57 (m, 6), 1.32 (d, J = 6.3 Hz, 3H); ESI-MS (−): $[M-H]^-$ m/z 505.2; ESI-MS (+): $[M+Na]^+$ m/z 529.1

Compound **3-R**: ^{1}H-NMR (300 MHz, pyridine-d_5): δ 6.95 (d, J = 2.1 Hz, 1H), 6.86 (d, J = 2.1 Hz, 1H), 6.52 (m, 1H), 6.34 (s, 1H), 6.09 (d, J = 14.7 Hz, 1H), 3.61 (m, 2H), 2.17–1.54 (m, 6H), 1.34 (d, J = 6.3 Hz, 3H); ESI-MS (−): $[M-H]^-$ m/z 505.1; ESI-MS (+): $[M+Na]^+$ m/z 529.2.

Compound **5-S**: ^{1}H-NMR (300 MHz, pyridine-d_5): δ 6.95 (s, 1H), 6.79 (s, 1H), 5.38 (m, 2H), 4.10 (m, 1H), 3.96 (overlap, 1H), 3.84 (overlap, 1H), 3.63 (overlap, 1H), 2.33 (m, 3H), 2.16 (m, 3H), 1.87 (m, 1H), 1.72 (m, 1H), 1.29 (d, J = 6.5 Hz, 3H); ESI-MS (−): $[M-H]^-$ m/z 549.1; ESI-MS (+): $[M+H]^+$ m/z 550.8, $[M+Na]^+$ m/z 572.7.

Compound **5-R**: ^{1}H-NMR (300 MHz, pyridine-d_5): δ 6.95 (s, 1H), 6.80 (s, 1H), 5.37 (m, 2H), 4.10 (m, 1H), 3.95 (overlap, 1H), 3.84 (overlap, 1H), 3.63 (overlap, 1H), 2.36 (m, 3H), 2.21 (m, 3H), 1.91 (m, 1H), 1.79 (m, 1H), 1.21 (d, J = 6.2 Hz, 3H); ESI-MS (−): $[M-H]^-$ m/z 549.2; ESI-MS (+): $[M+H]^+$ m/z 550.8, $[M+Na]^+$ m/z 572.9.

1. Wang S, et al. (2008) Functional characterization of the biosynthesis of radicicol, an Hsp90 inhibitor resorcylic acid lactone from *Chaetomium chiversii*. *Chem Biol* 15(12): 1328–1338.
2. Udwary DW, Merski M, Townsend CA (2002) A method for prediction of the locations of linker regions within large multifunctional proteins, and application to a type I polyketide synthase. *J Mol Biol* 323(3):585–598.
3. Zeng J, Valiente J, Zhan J (2011) Specific inhibition of the halogenase for radicicol biosynthesis by bromide at the transcriptional level in *Pochonia chlamydosporia*. *Biotechnol Lett* 33(2):333–338.
4. Zhan J, et al. (2004) A new anthraquinone and cytotoxic curvularins of a *Penicillium sp*. from the rhizosphere of *Fallugia paradoxa* of the Sonoran desert. *J Antibiot (Tokyo)* 57(5):341–344.
5. Bicalho B, Gonçalves RA, Zibordi AP, Manfio GP, Marsaioli AJ (2003) Antimicrobial compounds of fungi vectored by *Clusia* spp. (Clusiaceae) pollinating bees. *Z Naturforsch C* 58(9–10):746–751.
6. Greve H, et al. (2008) Apralactone A and a new stereochemical class of curvularins from the marine fungus *Curvularia* sp. *Eur J Org Chem* 2008(30):5085–5092.
7. Dai J, et al. (2010) Curvularin-type metabolites from the fungus *Curvularia* sp. isolated from a marine alga. *Eur J Org Chem* 2010(36):6928–6937.

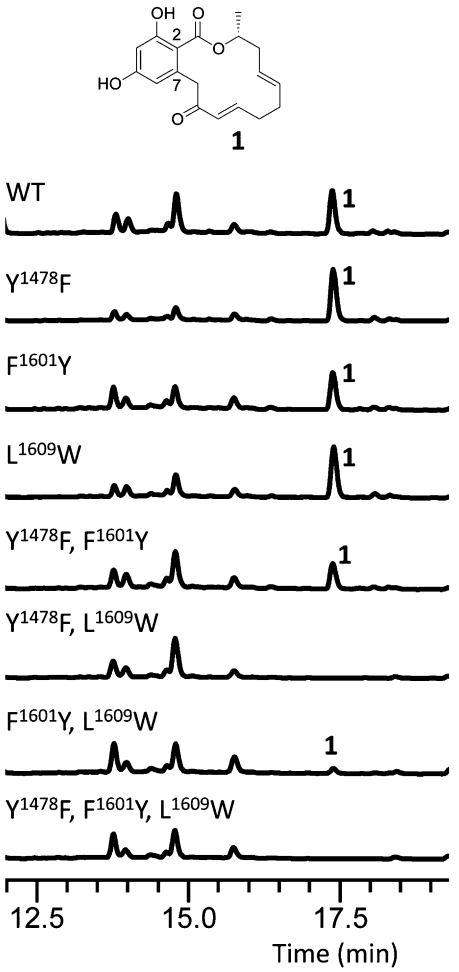

Fig. S1. Reprogramming first-ring cyclization regiospecificity by site-directed mutagenesis. Product profiles (HPLC traces recorded at 300 nm) of *S. cerevisiae* BJ5464-NpgA (1, 2) cotransformed with YEpCcRADS1 and the YEpCcRADS2 derivatives with the indicated mutations (*SI Materials and Methods*).

1. Ma SM, et al. (2009) Complete reconstitution of a highly reducing iterative polyketide synthase. *Science* 326(5952):589–592.
2. Zhou H, Qiao K, Gao Z, Vederas JC, Tang Y (2010) Insights into radicicol biosynthesis via heterologous synthesis of intermediates and analogs. *J Biol Chem* 285(53):41412–41421.

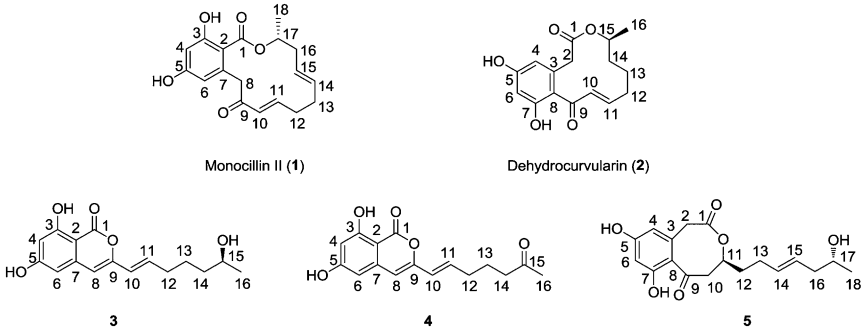

Fig. S2. Chemical structures of **1–5**.

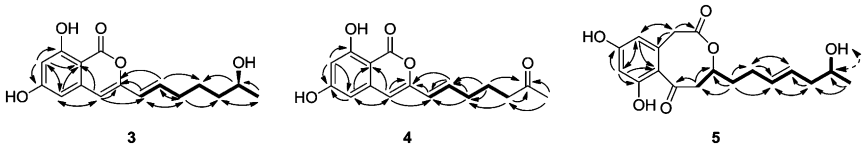

Fig. S3. Key HMBC (⟶), ^{1}H-^{1}H-COSY (▬), and ROESY (⇠⇢) correlations for **3–5**.

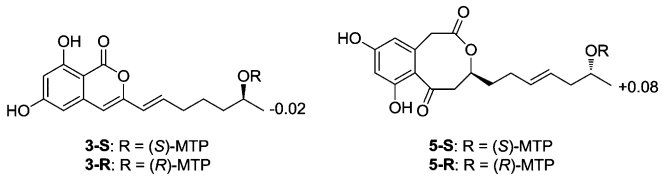

Fig. S4. Δδ-Values [Δδ (ppm) = $\delta_S - \delta_R$] obtained for (*S*)- and (*R*)-α-methoxy-α-(trifluoromethyl)phenylacetic acid esters of **3** and **5**.

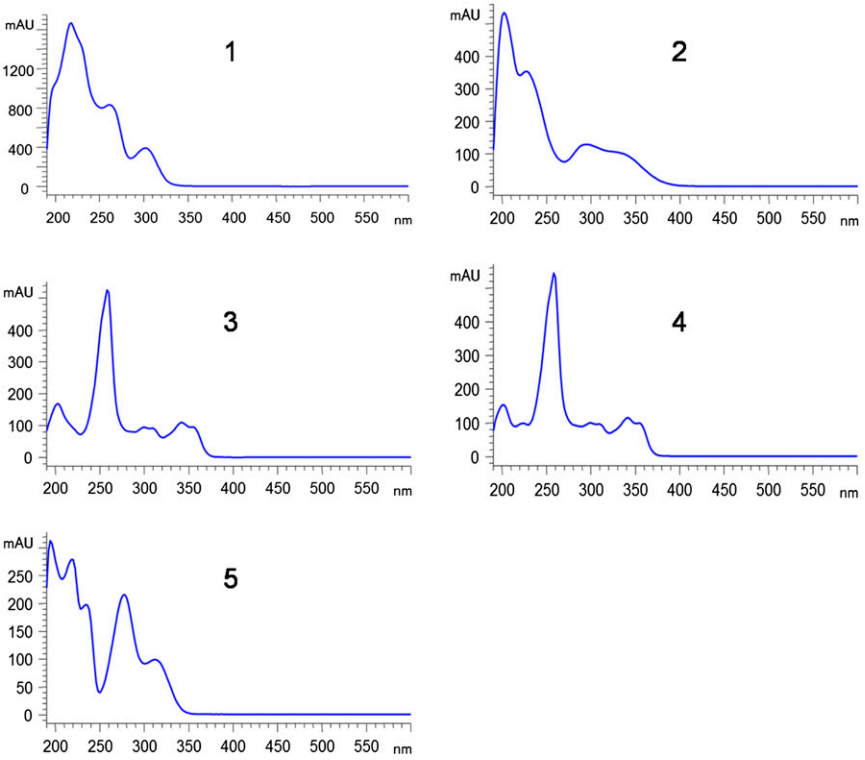

Fig. S5. The UV spectra of **1–5**.

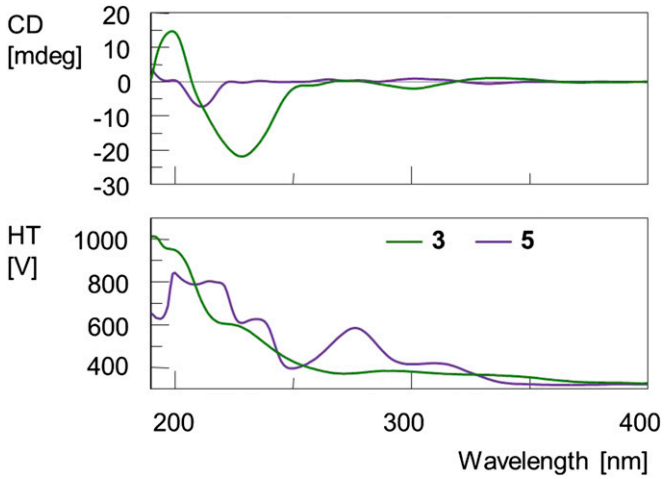

Fig. S6. The CD spectra of **3** and **5**.

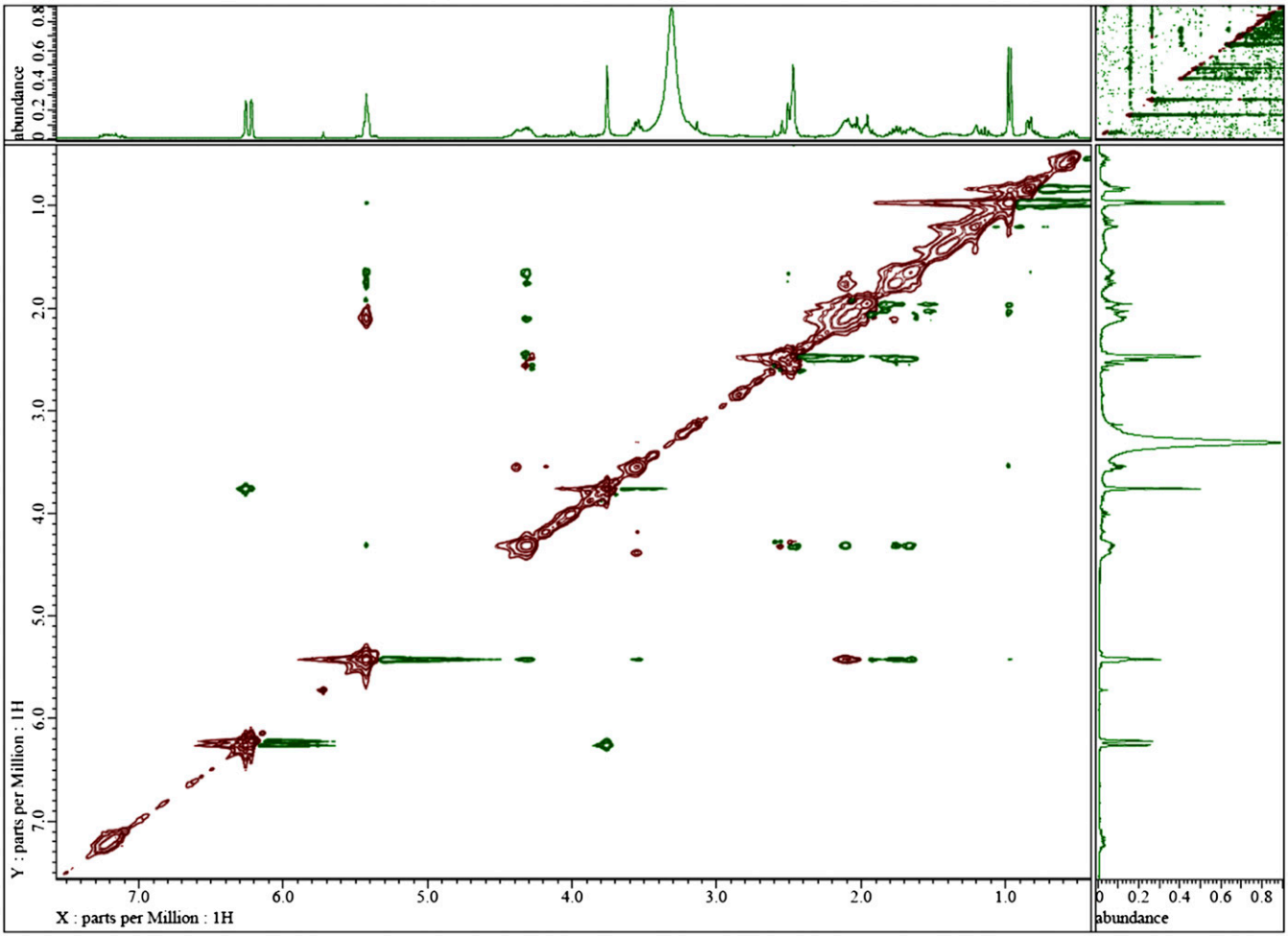

Fig. S7. The ROESY NMR spectrum of **5** (in DMSO-d_6).

Table S1. NMR data for 3–5

	3		4		5	
No.	δ_C	δ_H	δ_C	δ_H	δ_C	δ_H
1	165.9		163.9		172.5	
2	98.7		99.4		40.2	3.76 (s, 2H)
3	163.6		165.5		140.0	
4	104.5	6.29 (s, 1H)	105.4	6.20 (s, 1H)	112.7	6.26 (s, 1H)
5	166.0		167.3		163.4	
6	103.0	6.31 (s, 1H)	104.2	6.33 (s, 1H)	102.3	6.22 (s, 1H)
7	140.1		139.9		164.5	
8	101.4	6.34 (s, 1H)	102.5	6.56 (s, 1H)	114.8	
9	152.0		151.6		191.7	
10	121.9	6.13 (d, 1H, 15.9)	122.8	6.14 (d, 1H, 15.5)	43.1	2.51 (m, 2H)
11	136.0	6.51 (dt, 1H, 15.9, 7.2)	135.6	6.33 (m, 1H)	76.8	4.32 (m, 1H)
12	32.3	2.24 (m, 2H)	31.8	2.27 (m, 2H)	34.2	1.64 (m, 1H) 1.74 (m, 1H)
13	24.8	1.32 (m, 2H)	22.8	1.61 (m, 2H)	29.1	2.10 (m, 2H)
14	38.3	1.61 (m, 2H)	42.5	2.42 (m, 2H)	131.2	5.38 (m, 1H)
15	67.0	3.74 (m, 1H)	208.8		128.3	5.38 (m, 1H)
16	22.2	1.14 (d, 1H, 6.2)	29.8	2.01 (s, 3H)	42.8	1.98 (m, 1H)
17					66.5	3.55 (m, 1H)
18					23.5	0.98 (d, 3H, 8.2)
17-OH						4.38 (brs)

^{1}H (300 MHz) and ^{13}C NMR (75 MHz) data for **3–5** (**3** in CD_3OD and **4** and **5** in DMSO-d_6; *J* in Hertz and δ in parts per million).

Table S2. PCR primers used in this study

Primer name	Sequence
At_PT_Del_Dn_F	5′-AGTCGGCAAGCTGTGGCCGTCGC-3′
At_PT_Del_Dn_R (NheI)	5′-TACGCGTGCATGGCGACATGGTACG-3′
At_PT_Del_Up_F (AgeI)	5′-CCGGTGGCATCAACTCTGCTCGGAT-3′
At_PT_Del_UP_R	5′-ACGGCCACAGCTTGCCGACTCCCGGACCCAGTGACTGG-3′
At_PT_F	5′-CCGCTCGTCTCGACCTGCGC-3′
At_PT_p_F(KpnI)	5′-ATCGGTACCCTCACTAAAGGGAACAAAGC-3′
At_PT_p_R	5′-GCAGGTCGAGACGAGCGGATGAAGCTTGTCGTCATCGTC-3′
At_PT_R	5′-CATCTGCATCAGCCGGTCATGATCTTTAGACCTCGACGGC-3′
At_PT_t_F	5′-ATGACCGGCTGATGCAGATG-3′
At_PT_t_R (HpaI)	5′-TTCGTTAACAAAGATATGCTTCGAGGGGAGCAAAAAGTAG-3′
At_PT_to_Cc_F	5′-CCGCTCGTCTCGACCTGC-3′
At_PT_to_Cc_R	5′-TTTCTTGGGCGCTGTGGGGACCTCGACGGCTTTCTTG-3′
At_PT_Up_R	5′-CAGGTCGAGATCATTTGCTGCCCGGACCCAGTGACTGG-3′
Cc_PT_Del_Dn_F	5′-CCCACAGCGCCCAAGAAATCTGC-3′
Cc_PT_Del_Dn_R (BglII)	5′-ATGCACAGCAGCCTGTCGCCC-3′
Cc_PT_Del_Up_F (Bsu36I)	5′-CTGGCCGACCCAATCTGGCTCG-3′
Cc_PT_Del_Up_R	5′-AGATTTCTTGGGCGCTGTGGGCGCTGTAGGTGTAGCAGC-3′
Cc_PT_F	5′-CAGCAAATGATCTCGACCTGTGCAC-3′
Cc_PT_p_F (EcoRI)	5′-ATAGAATTCGGATCCATTTAGCGGCC-3′
Cc_PT_p_R	5′-CAGGTCGAGATCATTTGCTGATGAAGCTTGTCGTCATCGTC-3′
Cc_PT_R	5′-CCGTCTTGTGCGGCAGGCCAGATCTTTACGTCGCATCCTC-3′
Cc_PT_t_F	5′-GGCCTGCCGCACAAGACGG-3′
Cc_PT_t_R (HpaI)	5′-TTCGTTAACAAAGATATGCTTCGAGCTCGGTACCCTCGAG-3′
Cc_PT_to_At_F	5′-CAGCAAATGATCTCGACCTG3′
Cc_PT_to_At_R	5′-GCGACGGCCACAGCTTGCCGACTCGTCGCATCCTCCTTTTTCTC-3′
Cc_PT_Up_R	5′-GCAGGTCGAGACGAGCGG CGCTGTAGGTGTAGCAGC-3′
F332_F	5′-CCATGAAATCAGCAACGCAACGC-3′
F332Y_R	5′-TGCGTTGCTGATTTCATGGTACTCCAGACCGGAACACTGGGC-3′
L340_R	5′-CGTTGCGTTGCTGATTTCATGGAACTC-3′
L340W_F	5′-ATGAAATCAGCAACGCAACGTGGAAACAGGTTCTCTCTGGTGGC-3′
Phe198Tyr319_R	5′-AGGTCACCCGGGGGAGTTGGTG-3′
Phe198Y_R	5′-TGCCTCGTCGACGCCCTGGTAATCCGTGCTGAACTCGACTG-3′
RADS1_Dn_F	5′-ATGAGAGGCTTGTCGAGCTCGTCCGCATGGCAATAC-3′
RADS1_Dn_R (PmeI)	5′-GTCCGTTTAAACCTCACGCAGCCAACCCCACCAGC-3′
RADS1_Up_F (NdeI)	5′-CATCATATGCCATCAGCAACTGGAAAC-3′
RADS1_Up_R	5′-CTCGACAAGCCTCTCATGCGCG-3′
RADS2_F (NdeI)	5′-CATCATATGTCTAGGCTACCACAGAAGACC-3′
RADS2_R (PmeI)	5′-GTCCGTTTAAACCTCAATCCATCAAACCGTCTC-3′
Trp327_F	5′-CAGGAACTCCCCCGGGTGACCTGG-3′
Trp327L	5′-AACTCCCCCGGGTGACCTTGAAGCATGTTCTTGATGGGC-3′
Tyr319F_F	5′-CAGTCGAGTTCAGCACGGGATTACCAGGGCGTCGACGAGGC-3′
TYR319F_R	5′-TCACCCGGGGGAGTTCCTGAAACCGGAGGTCAATACATTGC-3′
Y209_F	5′-CAAGTGCATCAAAGAGGCGTACGTATCC-3′
Y209F_R	5′-ACGCCTCTTTGATGCACTTGAACTGGGAGTCGTACTCGAC-3′
Y319_R	5′-TCACCCGGGGGAGTTCCTGATACCGGAGGTCAATACATTGC-3′
Y332_F	5′-CCATGAAATCAGCAACGCAACGC-3′